RSC Advances

PAPER

View Article Online
View Journal | View Issue

Cite this: *RSC Adv.*, 2018, **8**, 40804

Removal of arsenic(v) from aqueous solutions using sulfur-doped Fe_3O_4 nanoparticles†

Junhui Liu,[a] Long Kong,*[a] Xueqiong Huang,[a] Min Liu[a] and Liang Li*[ab]

Received 20th October 2018
Accepted 22nd November 2018

DOI: 10.1039/c8ra08699k

rsc.li/rsc-advances

In this study, magnetic sulfur-doped Fe_3O_4 nanoparticles (Fe_3O_4:S NPs) were applied as adsorbents for the removal of As(v). Fe_3O_4:S NPs were fabricated by a two-step route, which included low-temperature mixing and high-temperature sintering. The as-prepared Fe_3O_4:S NPs could effectively remove As(v) under a wide pH range of 2–10 and presented a high As(v) adsorption capacity of 58.38 mg g^{-1}, which was much better than undoped Fe_3O_4 nanoparticles (20.24 mg g^{-1}). Adsorption experiments exhibited a pseudo-second-order model of adsorption kinetics and a Langmuir isotherm model of adsorption isotherms. Additionally, the coexisting ions such as NO_3^-, SO_4^{2-}, and CO_3^{2-} had no significant effect on As(v) adsorption and the adsorbent worked well in actual smelting wastewater. XPS and FTIR spectra of Fe_3O_4:S NPs before and after As(v) adsorption showed that Fe–OH groups played a significant role in the adsorption mechanisms. Moreover, the magnetic Fe_3O_4:S NPs adsorbents after adsorption could be rapidly separated from wastewater with an external magnetic field. Therefore, Fe_3O_4:S NPs could be an ideal candidate for the removal of As(v) from water.

1. Introduction

Arsenic is a persistent and toxic metalloid existing in the aquatic environment.[1–3] Arsenic may cause poisoning and death in humans as a result of contaminated water.[4–7] Recently, arsenic contamination problems were reported in India, Chile, Bangladesh, Vietnam, and other parts of the world.[8–10] In China, chronic arsenic exposure has caused very severe health problems.[11–13] Nearly 14.6 million people are exposed to contaminated water with arsenic concentration of 0.03 mg L^{-1} or higher every day.[14]

Varieties of technologies, such as coagulating sedimentation by CaO,[15] ion exchange,[16] and adsorption[17] have been used to remove arsenic from water. In spite of the low cost of coagulation process, it produces bulky sludge, and furthermore, the arsenic level in the water after treatment could not reach the strict standard of World Health Organization (WHO).[18] The problems of ion exchange process including high cost and the difficulty of regeneration have prevented it from wide application. On the contrary, adsorption process seems to be a promising technology because of the less sludge producing operation and high removal efficiency.[19,20] A lot of adsorbents have been developed to efficiently remove As(v) from water in the recent years.[21–29] As a sort of cheap adsorbents, iron oxides have been used for arsenic removal because of iron's affinity to inorganic arsenic species.[30] However, in certain situations, iron oxide presents low arsenic adsorption capacity, long adsorption process, and only works in a narrow pH range, which have greatly limited its application.[31,32] Hence, specific strategies such as surface modification and elements doping have attracted attentions to conquer these weaknesses.

In this study, sulfur-doped Fe_3O_4 nanoparticles (Fe_3O_4:S NPs) with excellent adsorption capacity and separation properties[33] were used for the removal of As(v) from water. Compared with undoped Fe_3O_4 NPs, the sulfur-doped nanoparticles exhibited a widely applicable pH range of 2–10 for As(v) removal. The prepared Fe_3O_4:S NPs were characterized using X-ray diffraction (XRD), transmission electron microscope (TEM), energy dispersive X-ray fluorescence (ED-XRF), Fourier transform infrared (FTIR), vibrating sample magnetometer (VSM), and X-ray photoelectron spectroscopy (XPS) analyses. The adsorption properties of Fe_3O_4:S NPs were investigated including the effects of initial pH, adsorption kinetics, adsorption isotherms, and the effects of coexisting ions. On account of these results, the possible mechanisms for the removal of As(v) were discussed.

2. Materials and methods

2.1 Materials and preparation

Sodium arsenate heptahydrate ($Na_2HAsO_4 \cdot 7H_2O$), iron(III) nitrate nonahydrate ($Fe(NO_3)_3 \cdot 9H_2O$), 1-butylamine, and

[a]School of Environmental Science and Engineering, Shanghai Jiao Tong University, 800 Dongchuan Road, Shanghai 200240, China. E-mail: liangli117@sjtu.edu.cn; longmao88@sjtu.edu.cn

[b]Shanghai Institute of Pollution Control and Ecological Security, 1239 Siping Road, Shanghai 200092, China

† Electronic supplementary information (ESI) available: XRD patterns of Fe_3O_4 NPs and Fe_3O_4:S NPs. EDX patterns of Fe_3O_4 NPs and Fe_3O_4:S NPs. See DOI: 10.1039/c8ra08699k

thiourea were supplied by Aladdin Chemical (Shanghai, China). All the chemicals were of analytical reagent grade and were used without any further purification. A 50 mg L^{-1} As(v) stock solution was prepared by dissolving 104.12 mg $Na_2HAsO_4 \cdot 7H_2O$ into 500 mL of distilled water (DI) (>18 MΩ cm). As(v) solution was prepared by diluting As(v) stock solution to a given concentration with distilled water. The industrial wastewater sample was taken from a smelting plant located in Hubei, China.

Fe_3O_4:S NPs were synthesized based on our previous report.[33] Typically, 60 mmol of thiourea and 20 mmol of $Fe(NO_3)_3$ were dissolved into 100 mL 1-butylamine, separately. After ultrasonic dispersion, the two solutions were mixed in a 250 mL three-neck flask under stirring. The mixture was heated to 60 °C with continuous stirring for 2 h in the atmosphere of flowing nitrogen. After cooling it to room temperature, the dark brown colored product was washed with methanol and acetone several times and was dried in a vacuum oven for 1 h at 60 °C. Then, the product was sintered at 300 °C for 2 h in the atmosphere of flowing nitrogen, and it was labeled as Fe_3O_4:S. For comparison, bare Fe_3O_4 NPs were prepared following the same procedure without the addition of thiourea. To prove that the Fe_3O_4 NPs and Fe_3O_4:S NPs were successfully prepared, XRD spectra and EDX spectra were recorded and provided in ESI (Fig. S2 and S4).†

2.2 Adsorption experiments

Adsorption experiments were conducted by adding adsorbents into As(v) solutions and stirring them continuously. At certain time intervals, the solutions were sampled and filtered through a 0.22 μm membrane to analyze the concentration of As(v). From the obtained results, the effects of initial pH on As(v) adsorption, adsorption kinetics, adsorption isotherms, and the effects of competing ions were studied.

The effect of initial solution pH on As(v) adsorption was investigated to determine the optimum pH of As(v) adsorption. The initial pH of the solutions was adjusted from 2 to 10 using 0.1 M HCl and NaOH. The as-prepared adsorbent (30 mg) was added to 60 mL of As(v) solution (20 mg L^{-1}) under continuous stirring at 30 °C for 24 h.

Adsorption kinetic experiments were conducted under the following conditions: The initial pH was set to the obtained optimum value. The as-prepared adsorbent (50 mg) was added to 100 mL of As(v) solution (20 mg L^{-1}) under continuous stirring at 30 °C for 24 h. Samples were gathered at certain intervals.

For Adsorption isotherm experiments, the concentrations of As(v) solutions were adjusted ranging from 5 mg L^{-1} to 50 mg L^{-1}. The as-prepared adsorbent (20 mg) was added to 40 mL of As(v) solution under continuous stirring at 30 °C. Samples were taken after 24 h.

To investigate the influence of coexisting ions, 20 mg of adsorbent was added to 40 mL of As(v) solution (30 mg L^{-1}) containing competing ions of NO_3^-, PO_4^{3-}, SO_4^{2-}, and CO_3^{2-} under continuous stirring (30 °C, 24 h). The concentrations of the competing ions were fixed at 0.4 mM and 0.8 mM to control the molar ratios of competing ions to As(v) at 1 and 2, respectively. Moreover, a control group was conducted under the same condition in the absence of competing ions.

The industrial wastewater samples (As 0.349 mg L^{-1}, Cu 0.095 mg L^{-1}, Ni 0.449 mg L^{-1}, 20 mL) from a smelting plant were mixed with the as-prepared adsorbent whose dosage range was from 0.25 g L^{-1} to 1 g L^{-1}. Under continuous stirring at 30 °C for 24 h, samples were compared with the original one. Chinese national standard (GB) of arsenic was also utilized as a reference.

The concentrations of As and total iron in the filtrates were analyzed using Inductive Coupled Plasma Emission Spectrometer (ICP-OES 5110, Agilent, USA) and Atomic Adsorption Spectrometer (ControlAA700, Analytik Jena AG, Germany). After adsorption, the adsorbents were separated from the solution by high-speed centrifuge, and then were dried in a vacuum oven at 60 °C to determine the adsorption mechanisms.

2.3 Characterization

The ED-XRF (EDX-720) analysis was conducted to determine the concentrations of Fe, O, and S in the resulted Fe_3O_4:S NPs. To analyze the crystalline structures of nanoparticles, the XRD measurement of Fe_3O_4:S adsorbent before and after adsorption was recorded on a Shimadzu XRD-6100 (Japan). Morphologies of the samples before and after adsorption were characterized using a TEM (JEM-2100F operating at 200 kV, Japan). FTIR spectra of Fe_3O_4:S NPs before and after adsorption were recorded by a Thermo Nicolet 6700 spectrometer (USA) over the wavelength range of 4000–400 cm^{-1}, using KBr as a reference. The magnetic measurement was conducted on a PPMS-9T (EC-II) of Quantum Design with a magnetic field up to 3 T. To measure the binding energies and atomic ratios, XPS analysis was performed on a Thermo Scientific Escalab 250Xi Photoelectron Spectrometer (USA) with a monochromatic Al Kα radiation source.

3. Results and discussion

3.1 Adsorption performance

3.1.1 Effect of pH on As(v) removal. The influence of initial pH on As(v) removal by Fe_3O_4:S NPs and Fe_3O_4 NPs was investigated under the pH range of 2–10. As shown in Fig. 1, the As(v) removal efficiency of Fe_3O_4:S NPs was nearly a constant value when the pH ranged from 2–9, which meant the As(v) adsorption capacity of Fe_3O_4:S NPs was almost not affected by the change of pH. In comparison, the optimum pH for Fe_3O_4 NPs to remove As(v) was 2, and As(v) removal efficiency decreased sharply when the pH increased. At a neutral pH, the As(v) removal efficiency of Fe_3O_4:S NPs was much higher than that of Fe_3O_4 NPs. Thus, Fe_3O_4:S NPs can be applied as an adsorbent at a neutral pH condition without losing the adsorption capacity or sacrificing the stability, herein the pH was chosen to be 6 for further adsorption experiments.

3.1.2 Adsorption kinetics. Fig. 2(a) shows the adsorption of As(v) by the as-prepared adsorbents as time dependent.[34] The adsorption of As(v) by Fe_3O_4:S NPs was rapid in the first 60 min,

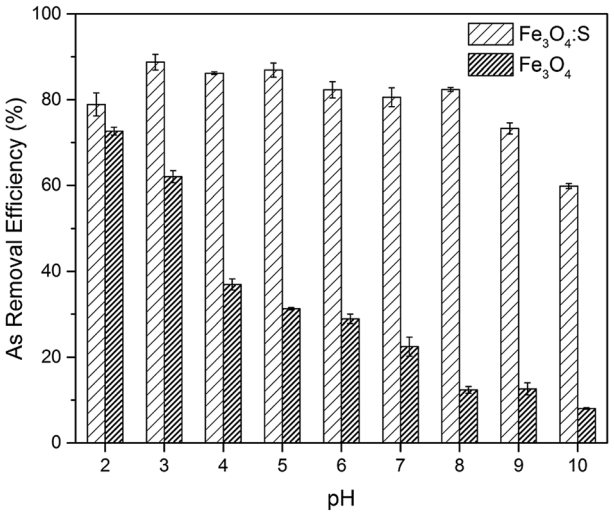

Fig. 1 The pH dependence for As(v) adsorption on Fe_3O_4:S NPs and Fe_3O_4 NPs. Experimental conditions: initial As(v) concentration was 20 mg L^{-1} (60 mL), adsorbent dosage was 30 mg, pH 2–10, contact time was 24 h, temperature was 30 °C.

and then it slowed down until reached equilibrium after 240 min with a maximum adsorption capacity of 42.17 mg g^{-1}. In comparison, the Fe_3O_4 NPs exhibited a much lower As(v) adsorption capacity of 19.64 mg g^{-1}. Obviously, the sulfur doping had a significant effect on the As(v) adsorption efficiency of Fe_3O_4:S NPs. We tested the Fe release kinetics of Fe_3O_4:S NPs and Fe_3O_4 NPs in pure water (Fig. 2(b)), and we found that the amount of Fe released from Fe_3O_4:S NPs was much more than that from Fe_3O_4 NPs. It was easy to understand, because the Fe–S is easier to break than Fe–O, which could release more Fe ions in water. However, in the treatment of wastewater containing As(v) ions, the release of Fe was suppressed as shown in Fig. 2(b) (blue line) because of the fast formation of Fe arsenates on the surface of adsorbent.

Pseudo-first-order model and pseudo-second-order model, as two different kinds of kinetic models, were utilized to simulate the kinetic experiments data of Fe_3O_4:S NPs and Fe_3O_4 NPs. The equations are mentioned below:[35,36]

$$\ln(q_e - q_t) = \ln q_e - k_1 t$$

$$\frac{t}{q_t} = \frac{1}{k_2 q_e^2} + \frac{1}{q_e} t$$

where q_t and q_e are the amount of As(v) adsorbed at any time t and the equilibrium time (mg g^{-1}), respectively. k_1 (min^{-1}) and k_2 (g mg^{-1} min^{-1}) refer to the rate constants of the two fitting models. From the two fitting models, we obtained the adsorption parameters and correlation coefficient (R^2) and listed them in Table 1. For both Fe_3O_4:S and Fe_3O_4 NPs, the plots of t/q_t *versus* t exhibited better linear dependence in the pseudo-second-order model (Fig. 3). As(v) adsorption capacity calculated using pseudo-second-order model was close to the experimental value, suggesting that chemical reaction was the critical rate-determining step.[37] In our experiments, chemisorption played a significant role in the removal of As(v) on Fe_3O_4:S NPs and Fe_3O_4 NPs.

3.1.3 Adsorption isotherm. Fig. 4(a) shows that the adsorption of As(v) is concentration dependent.[34] The plot illustrates the amount of As(v) adsorbed by the adsorbent (q_e) *versus* As(v) equilibrium concentration (C_e). As shown, q_e increased with the increase in C_e for both samples. Two adsorption isotherm models namely, the Langmuir and Freundlich isotherm models were used to analyze adsorption data of Fe_3O_4:S NPs and Fe_3O_4 NPs, respectively. The fitting equations of two isotherm models can be expressed as follows:[38,39]

$$\frac{C_e}{q_e} = \frac{C_e}{q_m} + \frac{1}{q_m K_L}$$

$$\ln\ q_e = \ln K_F + \frac{1}{n}\ \ln\ C_e$$

where C_e is the As(v) equilibrium concentration (mg L^{-1}), q_e is the amount of As(v) adsorbed at equilibrium (mg g^{-1}), q_m is the theoretical maximum adsorption capacity, K_L is the Langmuir constant relating to the energy of As(v) adsorption. K_F is the

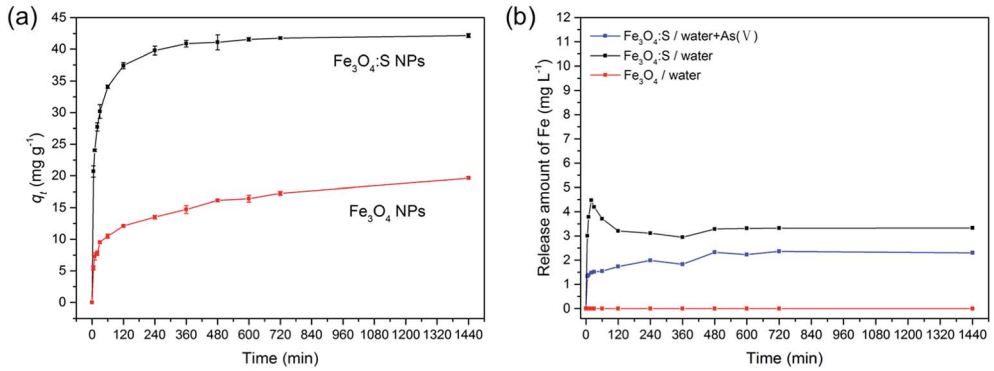

Fig. 2 (a) Adsorption kinetics of As(v) on Fe_3O_4:S NPs and Fe_3O_4 NPs; (b) Fe releasing kinetics of Fe_3O_4:S NPs and Fe_3O_4 NPs. Experimental conditions: initial As(v) concentration was 20 mg L^{-1} (100 mL), adsorbent dosage was 50 mg, pH 6, contact time was 24 h, temperature was 30 °C.

Table 1 Parameters related to kinetic models for As(v) adsorption

Adsorbent	Kinetic model	The rate constant	q_e (mg g^{-1})	R^2
Fe_3O_4:S	Pseudo-first-order model	5.67×10^{-3} (min^{-1})	16.08	0.906
	Pseudo-second-order model	1.93×10^{-3} (g mg^{-1} min^{-1})	42.44	0.999
Fe_3O_4	Pseudo-first-order model	2.44×10^{-3} (min^{-1})	12.51	0.915
	Pseudo-second-order model	8.35×10^{-4} (g mg^{-1} min^{-1})	19.51	0.988

theoretical maximum adsorption capacity, and n is related to the Freundlich adsorption intensity parameter. The fitting plots based on Langmuir and Freundlich isotherm models are shown in Fig. 4(b) and (c), and the parameters of Langmuir isotherm model are listed in Table 2. It is clear that the removal of As(v) by Fe_3O_4:S NPs and Fe_3O_4 NPs is better simulated by Langmuir model with a higher correlation coefficient (R^2) of 0.990 and 0.935, respectively. It indicated that the As(v) adsorption was mainly a monolayer sorption on the surfaces of Fe_3O_4:S and Fe_3O_4 NPs.[40] The theoretical maximum adsorption capacity (q_m) of Fe_3O_4:S NPs was 58.38 mg g^{-1}, which is much higher than that of Fe_3O_4 NPs (20.24 mg g^{-1}).

The feasibility of Langmuir isotherm adsorption can be expressed by separation factor, R_L, which is defined by $R_L = 1/(1 + K_L C_0)$,[41] where C_0 is the initial concentration of As(v). The calculated values of R_L in our experiments are 0.171 and 0.435 under the initial concentration of 5 mg L^{-1}, respectively, which are in the range of 0–1, indicating the type of favorable adsorption. A comparison of maximum adsorption capacity (q_m) of As(v) among Fe_3O_4:S NPs and other adsorbents are listed in Table 3.

Compared to Fe_3O_4 NPs, the adsorption capacity of Fe_3O_4:S NPs increased by 2.9 times, which was obvious and might attribute to sulfur doping. Compared to other iron-based adsorbents reported in recent years (Table 3), the distinct increase of adsorption capacity could be beneficial for their application.

3.1.4 Effect of competing ions on As(v) removal. Wastewater is always accompanied with a high salinity and hardness. Coexisting inorganic anions, such as phosphate, may compete with As(v) for binding sites of the adsorbent and affect As(v) removal.[46] As shown in Fig. 5, NO_3^- shows no apparent effect on the As(v) adsorption of Fe_3O_4:S NPs, on the contrary, PO_4^{3-} had significant inhibition on As(v) adsorption, while the addition of SO_4^{2-} and CO_3^{2-} decreased the As(v) adsorption capacity to a certain extent. The influence sequence of the four competing anions on As(v) adsorption is $PO_4^{3-} > SO_4^{2-} \approx CO_3^{2-} > NO_3^-$. The decrease of the As(v) adsorption capacity might be due to the competition for the binding sites between arsenate and phosphate.[34] These results demonstrated that Fe_3O_4:S could selectively remove As(v) in the presence of competing ions, which is a benefit for their practical application.

3.1.5 Removal of arsenic from industrial wastewater. As shown in Fig. 6, the industrial wastewater samples contained As, Ni, and Cu. With the addition of Fe_3O_4:S NPs, it was obvious that not only the concentration of As decreased significantly but also the concentrations of Ni and Cu. When the dosage of Fe_3O_4:S NPs was 0.25 g L^{-1}, the concentration of As in wastewater could reach the standard of 0.1 mg L^{-1} (Chinese national standard (GB) for secondary copper, aluminum, lead and zink industry,[47] GB31574-2015) and 0.05 mg L^{-1} (Environmental quality standards for surface water,[48] GB3838-2002). Moreover, Ni and Cu could also be adsorbed. Fe_3O_4:S NPs naturally contain two kinds of adsorption sites, *i.e.* Fe^{3+}/Fe^{2+} sites and S^{2-} sites. The former have excellent affinity to certain anions, such as AsO_3^{3-} and AsO_4^{3-}, while the S^{2-} sites can form strong soft–soft interaction (such as Pb–S bond and Cu–S bond) to remove heavy metal cations.[33] Thus, principally Fe_3O_4:S NPs could be an effective and promising adsorbent for wastewater treatment particularly for those smelting wastewater which usually contains As and other heavy metal ions.

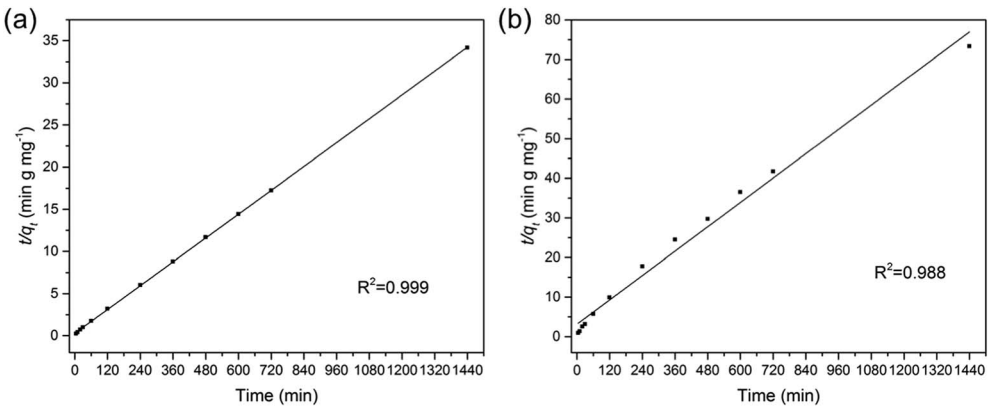

Fig. 3 (a) The pseudo-second-order model for As(v) adsorption on Fe_3O_4:S NPs; (b) the pseudo-second-order model for As(v) adsorption on Fe_3O_4 NPs.

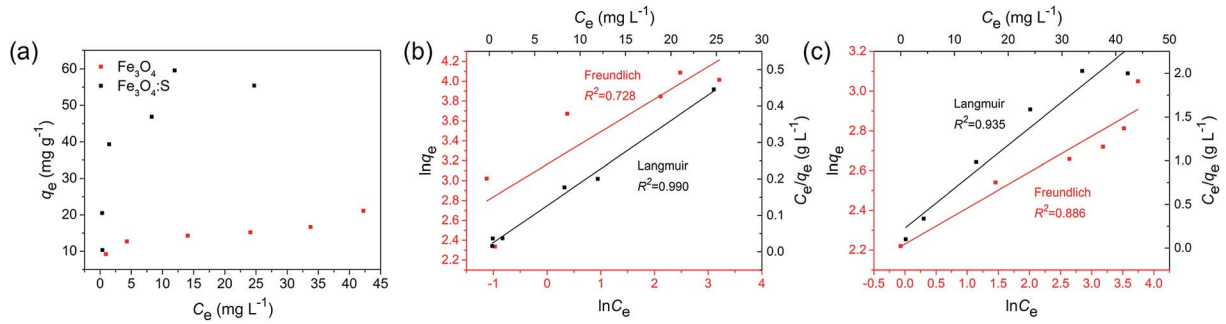

Fig. 4 (a) Adsorption isotherm of As(v) on Fe_3O_4:S NPs and Fe_3O_4 NPs; (b) the fitting of Langmuir and Freundlich models of Fe_3O_4:S NPs; (c) the fitting of Langmuir and Freundlich models of Fe_3O_4 NPs. Experimental conditions: initial concentration was 5–50 mg L^{-1} (40 mL), adsorbent dosage was 20 mg, pH 6, contact time was 24 h, temperature was 30 °C.

Table 2 Parameters related to Langmuir isotherm model for As(v) adsorption

Adsorbent	q_m (mg g^{-1})	K_L (L mg^{-1})	R^2
Fe_3O_4:S	58.38	0.971	0.990
Fe_3O_4	20.24	0.260	0.935

Table 3 Comparison of Langmuir adsorption capacity (q_m) for the adsorption of As(v) by adsorbents

Adsorbent	q_m (mg g^{-1})	Ref.
Chitosan-functionalized GO	71.9	42
Ascorbic acid-coated Fe_3O_4	16.56	43
Fe_3O_4@TiO_2	10.5	44
Fe_3O_4-HBC	3.35	45
Sulfur-doped Fe_3O_4	58.38	This work

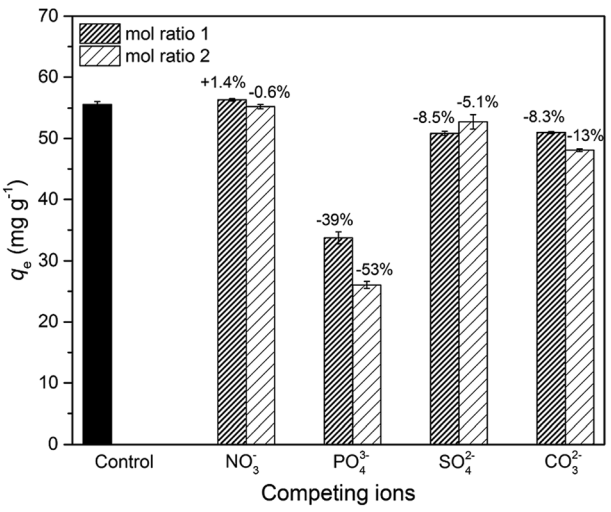

Fig. 5 The effect of competing anions on As(v) removal by Fe_3O_4:S NPs. Experimental conditions: initial As(v) concentration was 30 mg L^{-1} (40 mL), adsorbent dosage was 20 mg, pH 6, contact time was 24 h, temperature was 30 °C.

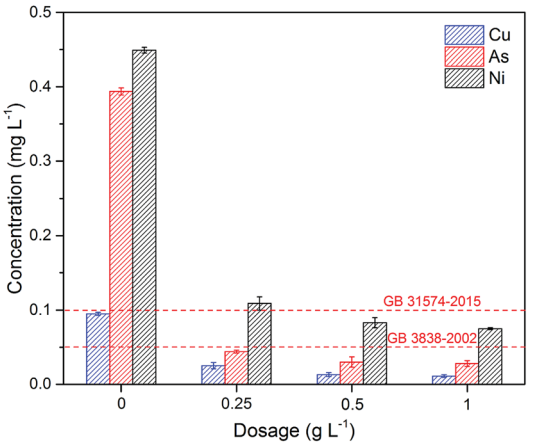

Fig. 6 The removal of As, Cu, and Ni by Fe_3O_4:S NPs in industrial wastewater. Experimental conditions: adsorbent dosage was 0.25–1 g L^{-1}, contact time was 24 h, temperature was 30 °C (GB 31574-2015:[47] Emission standards of pollutants for secondary copper, aluminum, lead, and zink industry; GB 3838-2002:[48] Environmental quality standards for surface water).

3.2 Adsorption mechanisms

To elucidate the major adsorption mechanisms of As(v) by Fe_3O_4:S NPs, XRD and TEM analyses were first conducted. Fig. 7 shows the XRD spectra of Fe_3O_4:S NPs before and after the As(v) adsorption. The peaks of Fe_3O_4:S NPs at 30.20°, 35.48°, 43.32°, 53.74°, 57.32°, and 62.78° correspond to the (220), (311), (400), (422), (511), and (440) lattice planes of magnetite Fe_3O_4 (JCPDS 19-0629), respectively, proving that the Fe_3O_4:S NPs were prepared successfully and were well-crystallized. The characteristic diffraction peaks of Fe_3O_4:S NPs slightly shifted to a smaller angle compared with Fe_3O_4 NPs (Fig. S2†). After As(v) adsorption, it is clear that compared with the Fe_3O_4:S NPs before adsorption, there was neither any shift in characteristic peaks nor a new peak occurred, which meant the well-crystallized nanoparticles were stable in the As(v) removal process.

The morphologies of Fe_3O_4:S NPs before and after As(v) adsorption are shown in Fig. 8. The well-crystallized nanoparticles had a size ranging from 4.34 nm to 13.46 nm with an average size of 7.84 nm. We didn't observe obvious changes on

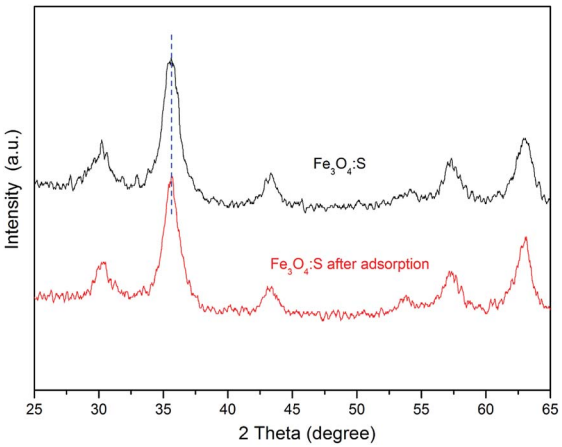

Fig. 7 XRD spectra of Fe_3O_4:S NPs before and after As(v) adsorption. Experimental conditions: initial As(v) concentration was 50 mg L^{-1} (100 mL), adsorbent dosage was 60 mg, pH 6, contact time was 24 h, temperature was 30 °C.

the morphologies and size distribution of these Fe_3O_4:S NPs after adsorption experiments, which is consistent with the XRD pattern. The lattice fringes with a *d*-spacing of 0.248 nm are assigned to the (311) planes of Fe_3O_4, and they remained almost unchanged after As(v) adsorption (Fig. 8(b) and (d)). The above XRD and TEM data indicate that the adsorption of As(v) most likely happened on the surface of Fe_3O_4:S NPs and didn't cause the crystal structure change. Thus, the FTIR analyses were conducted to check the surface changes of Fe_3O_4:S NPs.

The FTIR spectra of Fe_3O_4:S NPs before and after As(v) adsorption are shown in Fig. 9. For the sample before adsorption, it can be seen that the broad peak at wavenumbers 3402 cm^{-1} represents –OH stretching vibration, and the peak at 1621 cm^{-1} represents –OH bending vibration.[49] They exhibit certain changes at 3420 cm^{-1} and 1633 cm^{-1} after As(v) adsorption, respectively. A strong peak at 1041 cm^{-1} was observed from the sample before adsorption, which was assigned to the bending vibration of hydroxyl group (Fe–OH),[50,51] and it evidently weakened after adsorption, which might be attributed to the involvement of the Fe–OH groups in the adsorption process. The peak at 566 cm^{-1} represented Fe–O vibration.[29] After As(v) adsorption, it had a small shift at 577 cm^{-1}. In addition, a new peak at 822 cm^{-1} occurred, which corresponded to the stretching vibration of As–O.[51] According to these changes in Fe_3O_4:S NPs after As(v) adsorption, it was confirmed that As(v) was adsorbed onto the adsorbent and Fe–OH played a significant role in the adsorption process.[52]

In addition, we observed the surface structure of Fe_3O_4:S NPs before and after As(v) adsorption by XPS analysis. The XPS spectra of the survey scan and As3d are shown in Fig. 10(a) and (b), respectively. As shown in Fig. 10(a), the detected As species

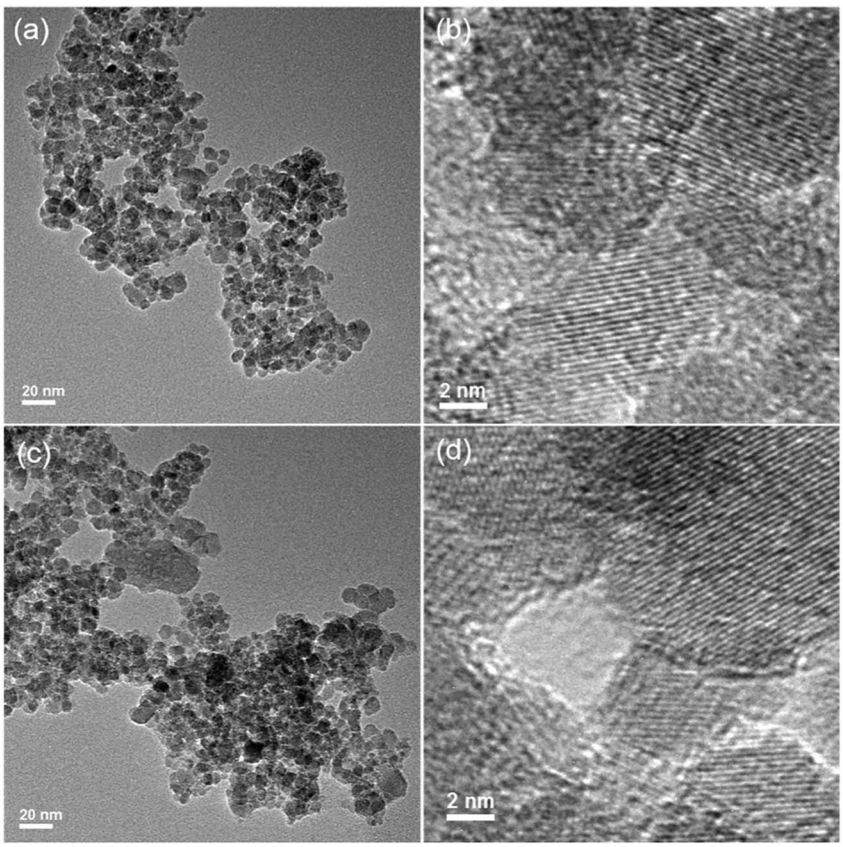

Fig. 8 TEM images of Fe_3O_4:S NPs before and after As(v) adsorption. (a and b) TEM and the corresponding HR-TEM image of Fe_3O_4:S NPs; (c and d) TEM image and the corresponding HR-TEM image of Fe_3O_4:S NPs after adsorption. Experimental conditions were the same as above.

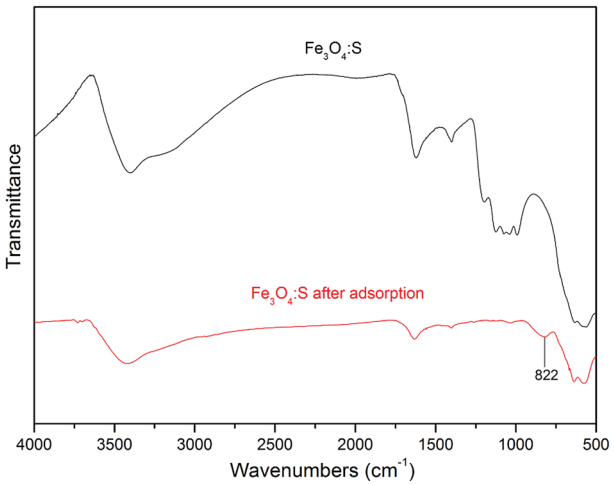

Fig. 9 FTIR spectra of Fe_3O_4:S NPs before and after As(v) adsorption. Experimental conditions were the same as above.

confirms that As was successfully adsorbed on the Fe_3O_4:S NPs. In the high resolution XPS spectra of As3d (Fig. 10(b)), the adsorbed As on Fe_3O_4:S NPs was mainly assigned to As(v), since the peak at 45.5 eV for As(v) is much higher than that at 44.9 eV for As(III). As shown in Fig. 10(a), the peak of S2p nearly disappeared after As(v) adsorption. The weight percentage of Fe, O, S, and As before and after adsorption measured by XRF are summarized in Table 4. As shown in Table 4, the amount of S in Fe_3O_4:S NPs after adsorption decreased to a large extent, which was consistent with the XPS spectrum. Considering the above-mentioned Fe release and the sulfur decrease in Fe_3O_4:S NPs after adsorption, we believe that the main role of sulfur was to break the magnetite structure in order to activate the Fe atoms and to acquire more Fe–OH absorption sites for As(v) adsorption.[53]

Magnetic properties of Fe_3O_4:S NPs and Fe_3O_4 NPs are presented in Fig. 11. The saturation magnetization of Fe_3O_4 NPs was 51.4 emu g^{-1}, and the saturation magnetization of Fe_3O_4:S NPs before and after adsorption were 37.1 emu g^{-1} and 39.9 emu g^{-1} with an external magnetic field at 3 T, respectively. The increase in saturation magnetization after adsorption might be attributed to the loss of sulfur during the adsorption process. Herein, Fe_3O_4:S NPs could be separated efficiently from aqueous solution after the adsorption of As(v) with an external magnetic field, which would be beneficial for their application. Separation experiments were conducted as shown in Fig. S1.† The adsorbent was dispersed in aqueous solution under continuous stirring. After adsorption, it took a long time for the adsorbent to precipitate naturally (Fig. S1(b)†). However, the separation process of magnetic Fe_3O_4:S nanoparticles was conducted effectively within a few minutes with the help of an external magnetic field (Fig. S1(c)†).

Table 4 Weight percentage of major components of Fe_3O_4:S before and after adsorption based on XRF analysis

Sample	Fe	O	S	As
Fe_3O_4:S	64.98	33.23	1.78	—
Fe_3O_4:S after adsorption	63.66	33.29	0.24	2.79

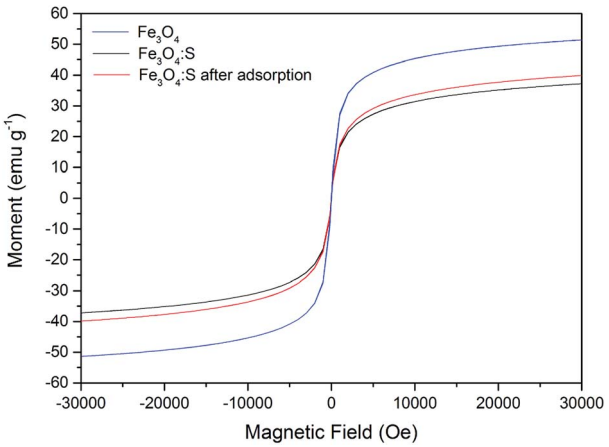

Fig. 11 Magnetization curves of Fe_3O_4:S before and after As(v) adsorption. Experimental conditions were the same as above.

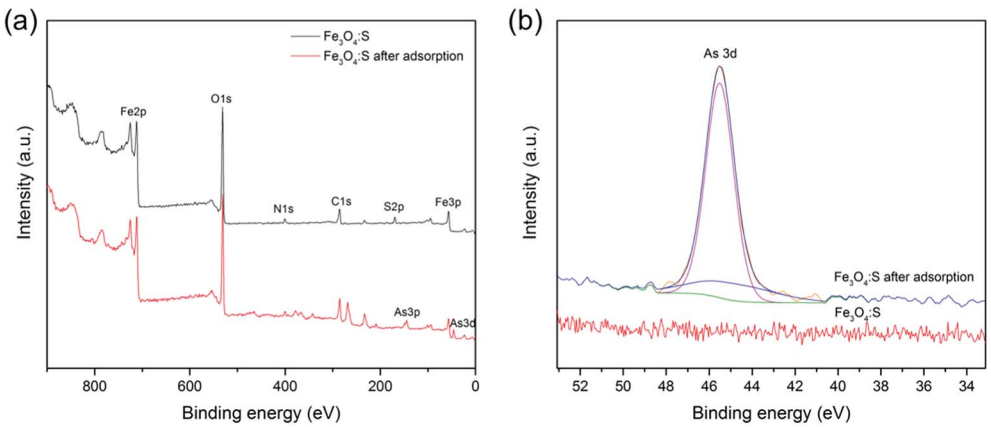

Fig. 10 (a) Full-range XPS spectra of Fe_3O_4:S before and after As(v) adsorption; (b) As XPS spectra of Fe_3O_4:S before and after adsorption. Experimental conditions were the same as above.

4. Conclusions

An iron-based adsorbent, sulfur-doped Fe_3O_4 nanoparticles were prepared for the removal of As(v). Batch adsorption experiments indicated that the Fe_3O_4:S NPs show a highly efficient removal of As(v) compared with undoped Fe_3O_4 NPs. The pseudo-second-order kinetic model fitted well ($R^2 = 0.999$) for As(v) adsorption. The Langmuir isotherm model was much more accurate ($R^2 = 0.990$) than the Freundlich model in describing the As(v) adsorption process. XPS and FTIR spectra of Fe_3O_4:S NPs before and after adsorption proved that the adsorption of As(v) was through the Fe–OH adsorption site, in which As(v) replaced the –OH group and formed stable Fe arsenates. The main role of sulfur doping was believed to affect the magnetite structure and activate the Fe atoms to acquire more Fe–OH absorption sites. Besides, the adsorbent could be efficiently separated from the As(v) solution with an external magnetic field. Thus, Fe_3O_4:S NPs have considerable potential for As(v) adsorption in wastewater.

Conflicts of interest

There are no conflicts to declare.

Acknowledgements

This work is supported by the Major National Science and Technology Special Project of Water Pollution Control and Remediation (2017ZX07202) and National Natural Science Foundation of China (21773155).

References

1 B. K. Mandal and K. T. Suzuki, *Talanta*, 2002, **58**, 201–235.
2 W. R. Cullen and K. J. Reimer, *Chem. Rev.*, 1989, **89**, 713–764.
3 P. Bhattacharya, A. H. Welch, K. G. Stollenwerk, M. J. McLaughlin, J. Bundschuh and G. Panaullah, *Sci. Total Environ.*, 2007, **379**, 109–120.
4 M. M. Hassan, *Arsenic in Groundwater: Poisoning and Risk Assessment*, Crc Press, 2018.
5 W. Ma, Y. Lin and Z. X. Feng, *China J. Mod. Med.*, 2018, **13**, 29–32.
6 S. Loewenberg, *Lancet*, 2016, **388**, 2336–2337.
7 S. Kapaj, H. Peterson, K. Liber and P. Bhattacharya, *Environ. Lett.*, 2006, **41**, 2399–2428.
8 J. Q. Jiang, *Water Sci. Technol.*, 2001, **44**, 89–98.
9 J. M. Borgoño, P. Vicent, H. Venturíno and A. Infante, *Environ. Health Perspect.*, 1977, **19**, 103.
10 M. Berg, H. C. Tran, T. C. Nguyen, H. V. Pham, R. Schertenleib and W. Giger, *Environ. Sci. Technol.*, 2001, **35**, 2621–2626.
11 P. N. Williams, M. Lei, G. Sun, Q. Huang, Y. Lu, C. Deacon and Y. G. Zhu, *Environ. Sci. Technol.*, 2009, **43**, 637–642.
12 H. A. Michael, *Science*, 2013, **341**, 852–853.
13 H. Guo, Y. Wang, G. M. Shpeizer and S. Yan, *J. Environ. Sci. Health, Part A: Toxic/Hazard. Subst. Environ. Eng.*, 2003, **38**, 2565–2580.
14 L. Zhang and C. Chen, *J. Hyg. Res.*, 1997, **26**, 310–313.
15 X. Guo, Z. Wu and M. He, *Water Res.*, 2009, **43**, 4327–4335.
16 L. Ruixia, G. Jinlong and T. Hongxiao, *J. Colloid Interface Sci.*, 2002, **248**, 268–274.
17 H. S. Altundoğan, S. Altundoğan, F. Tümen and M. Bildik, *Waste Manag.*, 2002, **22**, 357–363.
18 WHO, *Guidelines for drinking-water quality. Volume 2: health criteria and other supporting information*, 2nd edn, USA, 1996.
19 A. Audhya, M. Foti and S. D. Emr, *Int. Conf. Mater. Renewable Energy Environ.*, 2011, **2**, 1213–1216.
20 Y. Chammui, P. Sooksamiti, W. Naksata, S. Thiansem and O. A. Arqueropanyo, *Chem. Eng. J.*, 2014, **240**, 202–210.
21 USEPA, *Technologies and Costs for Removal of Arsenic from Drinking Water*, Books Llc, 2012.
22 Y. Meng, J. N. Wang, C. Cheng, X. Yang and A. M. Li, *Chin. Chem. Lett.*, 2012, **23**, 863–866.
23 S. Goldberg and C. T. Johnston, *J. Colloid Interface Sci.*, 2001, **234**, 204–216.
24 Y. Bai, T. Yang, J. Liang and J. Qu, *Water Res.*, 2016, **98**, 119–127.
25 M. L. Pierce and C. B. Moore, *Water Res.*, 1982, **16**, 1247–1253.
26 L. Yan, S. Hu and C. Jing, *J. Environ. Sci.*, 2016, **49**, 74–85.
27 N. Horzum, M. M. Demir, M. Nairat and T. Shahwan, *RSC Adv.*, 2013, **3**, 7828–7837.
28 H. H. Li, W. F. Yan, Q. Liang, E. Zheng-yang and K. J. Ge, *Nat., Environ. Pollut. Technol.*, 2017, **16**, 627–632.
29 H. Genç-Fuhrman, J. C. Tjell and D. McConchie, *Environ. Sci. Technol.*, 2004, **38**, 2428–2434.
30 G. T. Burstein, *Mineral. Mag.*, 1997, **61**, 740–741.
31 T. H. Hsia, S. L. Lo, C. F. Lin and D. Y. Lee, *Colloids Surf., A*, 1994, **85**, 1–7.
32 J. A. Muñoz, A. Gonzalo and M. Valiente, *Environ. Sci. Technol.*, 2002, **36**, 3405–3411.
33 X. Huang, L. Kong, S. Huang, M. Liu and L. Li, *Sci. China: Chem.*, 2018, **61**, 164–171.
34 Y. Zhang, M. Yang and X. Huang, *Chemosphere*, 2003, **51**, 945–952.
35 L. Kong, L. Yan, Z. Qu, N. Yan and L. Li, *J. Mater. Chem. A*, 2015, **3**, 15755–15763.
36 C. Ling, F. Q. Liu, C. Xu, T. P. Chen and A. M. Li, *ACS Appl. Mater. Interfaces*, 2013, **5**, 11808–11817.
37 Y. S. Ho and G. McKay, *Process Biochem.*, 1999, **34**, 451–465.
38 Y. Li, Q. Du, X. Wang, P. Zhang, D. Wang, Z. Wang and Y. Xia, *J. Hazard. Mater.*, 2010, **183**, 583–589.
39 M. M. Motsa, B. B. Mamba, J. M. Thwala and T. A. Msagati, *J. Colloid Interface Sci.*, 2011, **359**, 210–219.
40 M. Dastkhoon, M. Ghaedi, A. Asfaram, A. Goudarzi, S. M. Langroodi, I. Tyagi and V. K. Gupta, *Sep. Purif. Technol.*, 2015, **156**, 780–788.
41 G. Mckay, H. S. Blair and J. R. Gardner, *J. Appl. Polym. Sci.*, 1982, **27**, 3043–3057.
42 A. S. K. Kumar and S. J. Jiang, *J. Environ. Chem. Eng.*, 2016, **4**, 1698–1713.
43 L. Feng, M. Cao, X. Ma, Y. Zhu and C. Hu, *J. Hazard. Mater.*, 2012, **217**, 439–446.
44 J. Lan, *Res. Chem. Intermed.*, 2015, **41**, 3531–3541.

45 S. A. Baig, T. T. Sheng, C. Sun, X. Xue, L. Tan and X. Xu, *PLoS One*, 2014, **9**, e100704.
46 S. A. Wasay, S. Tokunaga and S. W. Park, *Sep. Sci. Technol.*, 1996, **31**, 1501–1514.
47 SEPA, *Emission standards of pollutants for secondary copper, aluminum, lead and zink industry (GB31574-2015)*, Beijing, 2015.
48 SEPA, *Environmental quality standards for surface water (GB3838-2002)*, Beijing, 2002.
49 J. D. Russell, *Clay Miner.*, 1979, **14**, 109–114.
50 J. T. Keiser, C. W. Brown and R. H. Heidersbach, *J. Electrochem. Soc.*, 1982, **129**, 2686–2689.
51 K. Nakamoto, *Infrared and Raman spectra of inorganic and coordination compounds*, 1978.
52 S. Tokunaga, M. J. Haron, S. A. Wasay, K. F. Wong, K. Laosangthum and A. Uchiumi, *Int. J. Environ. Stud.*, 1995, **48**, 17–28.
53 Y. Zhang, M. Yang, X. M. Dou, H. He and D. S. Wang, *Environ. Sci. Technol.*, 2005, **39**, 7246–7253.